Sensors and Materials, Vol. 38, No. 5 (2026) 2633–2652
MYU Tokyo

S & M 4459

Variational Autoencoder-optimized Soft Robot Deformation Controller for Reducing Surgical Invasiveness

Din-Yuen Chan,[1] Jhing-Fa Wang,[2] and Chien-I Chang[1*]

[1]Department of Computer Science and Information Engineering, National Chiayi University, No. 300, Syuefu Road, East District, Chiayi City 60004, Taiwan, R.O.C.
[2]Department of Electrical Engineering, National Cheng Kung University, No. 1, University Road, East District, Tainan City 70101, Taiwan, R.O.C.

(Received December 12, 2025; accepted April 20, 2026)

Keywords: soft robot, variational autoencoders, model predictive control, deformation control, minimally invasive surgery

The development of advanced soft robotics is crucial for delicate medical operations, as traditional rigid robots lack the flexibility required for such procedures. However, the application of nonlinear time-varying dynamics mechanisms to achieve accurate deformation control still faces challenges. In this study, we address the design of a surgical-tool deformation controller for minimally invasive procedures and propose a collaborative framework that integrates a variational autoencoder (VAE) with a two-dimensional time-varying model predictive controller (MPC). In our primary simulation, compared with the proportional integral derivative (PID), MPC results in improvements by reducing the convergence time by 50%, lowering deformation error by 75%, producing smoother control inputs, and consuming one-sixth the energy. Moreover, MPC demonstrates strong adaptability, stability, and high precision in dynamic operating conditions, thereby ensuring surgical safety, particularly when subjected to discrete external forces. To reduce the computational load in real-time optimization, the VAE is trained offline using MPC data, and subsequently generates the optimal control sequences while enhancing interpretability. The proposed VAE-enhanced soft-robot deformation controller, termed VAI-SDC, can achieve approximately 17% greater energy savings and higher control accuracy than standalone MPC. The experimental results demonstrate that VAI-SDC can attain precise, energy-efficient deformation control of surgical instruments in time-varying environments. As the utilization of VAI-SDC minimizes the invasiveness of surgery, it promises reliable robotic assistance for the safety of clinical applications.

1. Introduction

Soft robots, characterized by their compliance, adaptability, and biocompatible mechanical properties, hold great potential for biomedical applications such as minimally invasive surgery, targeted drug delivery, and tissue repair. Their small scale enables navigation through complex

*Corresponding author: e-mail: s1100311@mail.ncyu.edu.tw
https://doi.org/10.18494/SAM6122

ISSN 0914-4935
https://myukk.org/

biological environments with minimal tissue damage. Future research should address challenges in material durability, immune response, control strategies, and multifunctional integration to ensure reliability and clinical safety. Collaboration between engineers and medical professionals will be crucial to advance soft robots from experimental prototypes toward practical medical implementations, accelerating their transition from research laboratories to real-world healthcare applications.[1] Deformation prediction in soft robots has been explored through physical modeling and data-driven approaches. Euler–Bernoulli beam models and finite element analyses for pneumatic actuators[2] provide strong theoretical accuracy but suffer from high computational cost, parameter sensitivity, and poor adaptability to dynamic environments, limiting real-time use. Traditional machine learning methods, such as support vector machines and principal component analysis, have been applied to data-driven deformation pattern extraction but struggle with high-dimensional nonlinear dynamics. Recently, the enhanced variational autoencoder (VAE) module has demonstrated the ability to effectively learn complex input–output mappings and achieve robust deformation prediction without relying on explicit physical equations.

Unlike rigid robots, soft robots lack a unified control framework, and their nonlinear, time-varying dynamics pose major challenges for deformation regulation. Traditional approaches often rely on the proportional integral derivative (PID) and fuzzy control; thus, PID has been widely used owing to its simplicity, but it assumes fixed parameters. Generally speaking, the insufficient adaptability of classical methods leads to steady-state errors, overshoot, and oscillations while performing time-varying complex nonlinear deformation control in soft robots.

Autoencoders lack interpretability in latent spaces, and Kingma and Welling therefore proposed the VAE to integrate probabilistic graphical models with variational inference to enable the generation of high-quality data.[3] As a nonlinear dimensionality reduction approach, the VAE effectively learns latent representations to generate new data samples, thereby bridging deterministic and probabilistic modeling paradigms. Since its introduction, VAEs have been widely applied in various domains, including image caption generation,[4] medical data classification,[5] and traffic data reconstruction.[6] Furthermore, extensions such as the conditional VAE (CVAE) and multichannel VAE (MVAE) have enhanced generative controllability and source separation capabilities.[7] Despite these advantages, VAEs still face challenges related to computational demands and model interpretability.

For bilinear models, Bloemen *et al.* proposed the model predictive controller (MPC) based on discrete-time bilinear state-space models,[8] converting nonlinear optimization into quadratic programming, and achieved superior performance. Lou *et al.* applied predictive control to nonlinear stochastic partial differential equations (PDEs) to regulate state variance, manifested as surface roughness in thin-film growth.[9] Mahmood and Mhaskar extended MPC to nonlinear systems with input constraints,[10] enlarging the set of initial conditions to ensure closed-loop stability. Despite its advantages, MPC requires accurate dynamic models, making deformation control challenging in complex environments where solving PDE-based relationships is computationally prohibitive. To address this limitation, data-driven MPC methods have been explored, with VAE-enhanced MPC offering a lightweight solution for real-time deployment.

The proposed VAI-SDC integrates data-driven and model-based components with a VAE through a unified fusion architecture. Its framework consists of an offline learning phase, in which the VAE extracts mappings between external force patterns and optimal control inputs, thereby reducing computational load and latency. The learned representation is incorporated into MPC to enhance interpretability and prediction quality. During the online procedure, the VAE generates an initial control-parameter sequence, which is then refined by MPC in real time. This two-phase mechanism, termed VAE-MPC, effectively overcomes the limitations of PID-based control when managing highly nonlinear and time-varying deformation dynamics. As a result, the framework enables robust and efficient real-time deformation control for soft robotic systems.

2. Related Work

Traditional rigid robots, composed of hard components and mechanical joints, have long dominated industrial applications but remain limited in adaptability. In contrast, flexible bionic robots, inspired by organisms without rigid skeletons, achieve complex motions through intrinsic deformation. The Whitesides group at Harvard University introduced a fully soft, pneumatically driven quadruped made of silicone, capable of autonomous crawling and obstacle avoidance.[11] Presently, soft robotic technology has evolved toward dual-core applications—robust grasping and precision medicine. Because of their mechanical compliance, soft robots enable the safe manipulation of objects with diverse shapes and fragility.

Robotics has also entered the medical domain, with numerous interdisciplinary innovations combining mechanics, imaging, materials, and control theory. A significant milestone was the da Vinci surgical system, launched by Intuitive Medical, which integrates an operator console, robotic arms, and instrument modules. However, the development of purely rigid medical robots has progressed slowly, motivating the emergence of soft medical robotics to overcome these limitations. Ranzani *et al.* proposed an octopus-inspired variable-stiffness manipulator to address the dexterity constraints of traditional laparoscopic tools,[12] while soft grippers with compliant jaws minimize tissue damage during operation.[13]

Nevertheless, the complex deformation arising from interactions between soft surgical tools and biological tissues still challenges precision control, with approximately 23.5% of surgical complications attributed to improper instrument handling.[14] Although the da Vinci robotic system significantly enhances surgical accuracy and stability, its high cost restricts widespread clinical adoption. Consequently, the development of soft medical robots offers a promising path toward safer, more adaptable, and cost-effective solutions for next-generation minimally invasive surgery.

2.1 Soft robot modeling technology

Soft robot modeling is crucial for motion control tasks. Current modeling approaches can be generally classified into two categories: experimental modeling and theoretical modeling. Experimental modeling establishes input–output or behavioral relationships directly from data,

enabling fast construction at the cost of extensive experimental data. Theoretical modeling relies on physical laws to build mathematical models and offers high accuracy at the cost of heavy computation. Hybrid modeling integrates both advantages and has become an important direction in handling complexity and uncertainty in soft robot systems. However, the strong nonlinearity and coupling of soft robots still challenge accurate modeling and control. Practical applications require precise mechanical, kinematic, and dynamic models to predict deformation, stress, and motion behavior effectively.

This process is an important prerequisite for the design and control of soft robots, in which the modeling of soft robots follows three main principles.

(1) Simplify the complex problem as much as possible by eliminating insignificant factors, extracting the most essential features of the soft robot, and achieving dimensionality reduction in parametric characterization. In addition, simplify the nonlinear stress–strain relationship of the continuum material into a finite-degree-of-freedom parameter space, thereby reducing computational complexity from $O(n^3)$ to $O(n)$.
(2) Establish mathematical formulations after extracting the interaction relationships, such that equations and mathematical expressions can describe the stress distribution and deformation behavior of the soft robot.
(3) Specify the design objectives, which may include optimizing the robot's structure, developing control algorithms, predicting system behavior, or integrating these aspects into a unified modeling-and-control framework. The optimal design of a soft robot typically involves considerations such as control accuracy, energy consumption, deformation angle, and other relevant performance metrics.

Soft robot technology places increasing demands on structural materials, which differ fundamentally from those of rigid robots by emphasizing flexibility and adaptability. Soft robots often use low-modulus biomimetic materials that withstand large strain and maintain function under compression. Their mechanical properties directly influence deformation and controllability. Although distributed deformation offers theoretically infinite degrees of freedom, the nonlinear stress–strain behavior makes modeling difficult. Therefore, selecting functional soft materials capable of large deformation and understanding their deformation mechanisms are crucial for accurate modeling.

2.2 Common theoretical modeling methods

Typical soft robots use silicone materials for their excellent biocompatibility and elasticity. Zhou *et al.* developed a human-hand-like soft gripper with three flexible fingers and an adaptive palm,[15] capable of stretching several times its original length and recovering after unloading, demonstrating strong elasticity and reliable grasping performance. Such reversible large deformation behavior can be characterized by the Ogden model, whose strain energy density function W is shown as

$$W = \sum_{p=1}^{N} \left(\frac{\mu_p}{\alpha_p} \left(\lambda_1^{\alpha_p} + \lambda_2^{\alpha_p} + \lambda_3^{\alpha_p} - 3 \right) \right), \tag{1}$$

where λ_1, λ_2, and λ_3 are the principal stretches and indicate the degree of deformation of the material in the three main directions. μ_p and α_p are the material parameters shear modulus and nonlinear index, respectively. N is the number of terms in the model, usually selected in accordance with the complexity of the material and the fitting requirements of the experimental data.

Compared with the three-dimensional model, the one-dimensional simplified model can reduce the nonlinear hyperelastic constitutive relationship in three-dimensional space to a one-dimensional parameter space, enabling more efficient and concise simulation control. The piecewise constant curvature model (PCC) is a common one-dimensional simplified model. The soft robot continuum in three-dimensional space is abstracted into a spatial arc, and its curvature is approximately constant when it deforms.

2.3 Kinetic modeling of minimally invasive tool-lesion target contact system

Traditional minimally invasive surgery (MIS) is widely accepted owing to its known benefits, such as smaller wounds and less scarring. However, MIS is inherently limited by fixed incision points, and the rigid, expensive surgical instruments directly restrict the flexibility of operations. Soft robots lack traditional discrete joints, possessing, instead, infinite degrees of freedom (DoFs). The concept of finite approximation is employed to model this infinite DoF deformation of soft tools in minimally invasive surgery, using a segmented variable curvature space curve. Each approximated curve segment can be regarded as a structural 'element'. In a simplified control strategy, we may primarily consider the deformation of only a small section, such as the cutting edge part, to reduce complexity and focus on the area crucial for task execution. In engineering modeling, the curvature change in a small range of the curve is often ignored, and the straight line approximation is used to simplify the analysis.

When the scalpel's end effector contacts human tissue, it experiences significant deformation due to the initial force exerted by the tissue. This causes a deflection along the tangential direction at each point on the blade, with these deflection angles forming a deflection set. The proposed VAE is responsible for learning the mapping from the deflection angles to the initial force (i.e., the control input state). MPC then regulates the deflection angles to remain as close to zero as possible on the basis of the learned force. The dynamic model of a minimally invasive tool's end effector in contact with objects is illustrated in Fig. 1.

Set the modeling target to the dynamic equation of minimally invasive tool end-effector bending (simplified model). According to Lagrangian mechanics, the following is derived.

Because of the velocity of the center of mass $v_p = [\dot{x} + l\dot{\theta}\mathrm{coscos}\theta, -l\dot{\theta}\mathrm{sinsin}\theta]$, the kinetic energy of the system

$$T = \frac{1}{2}M\dot{x}^2 + \frac{1}{2}m\left(\dot{x}_p^2 + \dot{y}_p^2\right) = \frac{1}{2}M\dot{x}^2 + \frac{1}{2}m\left(\dot{x}^2 + l^2\dot{\theta}^2 + 2l\dot{x}\dot{\theta}\cos\cos\theta\right). \tag{2}$$

The potential energy of the system is

$$V = fy_p = fl\cos\cos\theta. \tag{3}$$

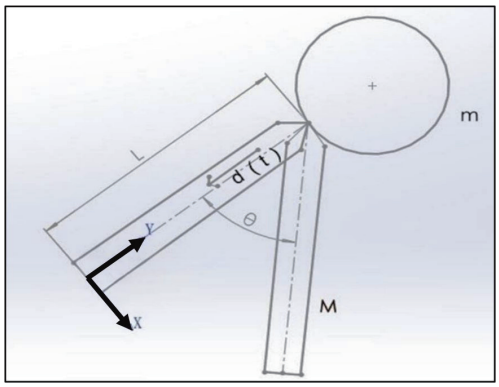

Fig. 1. (Color online) Dynamic model of a minimally invasive tool's end effector in contact with objects.

Thus, the Lagrangian quantity is

$$\mathcal{L} = T - V = \frac{1}{2}\left(M + m\right)\dot{x}^2 + ml\dot{x}\dot{\theta}\cos\cos\theta + \frac{1}{2}ml^2\dot{\theta}^2 - fl\cos\cos\theta. \tag{4}$$

Apply the Lagrangian equation as

$$\frac{d}{dt}\left(\frac{\partial \mathcal{L}}{\partial \dot{q}_i}\right) - \frac{\partial \mathcal{L}}{\partial q_i} = Q_i, \tag{5}$$

where q_i is generalized coordinates (x and θ) and Q_i is the generalized force (F and θ).

The kinetic equations of the system are

$$\left(M + m\right)\ddot{x} + ml\ddot{\theta}\cos\cos\theta - ml\dot{\theta}^2\sin\sin\theta = F, \tag{6}$$

$$ml^2\ddot{\theta} + ml\ddot{x}\cos\cos\theta - fl\sin\sin\theta = 0. \tag{7}$$

The specific symbols used and their meanings are shown in Table 1.

2.4 MPC

MPC is an advanced control strategy based on optimization theory and can be regarded as a method to apply optimization ideas under the control framework. It is widely used in the field of industrial process control and system optimization. In the control system, the driver and actuator, which belong to the physical implementation part of the control chain, are the underlying execution units of MPC. The combination of MPC control ideas forms a complete control framework. The focus of this paper is on the layout of the control layer, that is, the frame design of the MPC, as shown in Fig. 2.

Table 1
Symbols used in formulas.

Parameters	Description	Unit
M	Mass of the flexible portion of the minimally invasive tool end effector	kg
l	Length of the flexible portion of the minimally invasive tool end effector	m
m	Mass of the tissue under load	kg
θ	Deflection angle of the tool between the tissue and the end effector after force is applied	rad
x	Position of the minimally invasive tool end effector	m
F	Actuating force	N
g	Gravity acceleration	$M*S^2$
f	Time-varying force acting on the tool	N

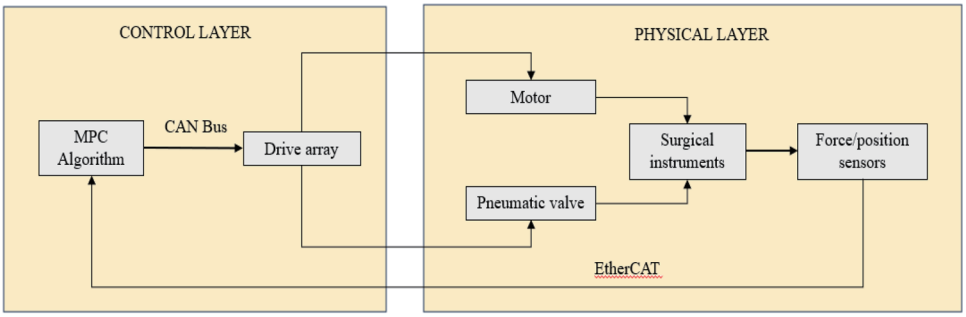

Fig. 2. (Color online) Complete deployment diagram of the control system.

The implementation of MPC optimal control strategy is based on the mathematical model of the system, which predicts the future output of the system, optimizes the control strategy at each moment online, and solves the optimal control input. Therefore, MPC is mainly divided into three parts, namely, predictive model, rolling optimization, and feedback correction.

Prediction is based on a known control signal and the simulation of the signal sequence of the future moment to the front end of the system. Considering the dynamic characteristics of the minimally invasive tool end effector in the time-varying environment, the system state vector $z = [x\ \theta\ \dot{x}\ \dot{\theta}]$ and control input $u = F$ are established, and the nonlinear equation of state is shown as

$$\dot{z} = f(z) + g(z)u, \tag{8}$$

where $f(z)$ is the nonlinear drift term (when there is no input) and $g(z)$ is the input coupling term.

$$\begin{aligned} \dot{z} = &\begin{bmatrix} \dot{x} & \dot{\theta} & \dfrac{ml\dot{\theta}^2 \sin\sin - mg\sin\sin s\cos}{M + m(\sin\sin)^2} & \dfrac{(M+m)g\sin\sin - ml\dot{\theta}^2 \sin\sin s\cos}{l\left[M + m(\sin\sin)^2\right]} \end{bmatrix} \\ &+ \begin{bmatrix} 0 & 0 & \dfrac{1}{M + m(\sin\sin\theta)^2} & -\dfrac{\cos\cos\theta}{l\left[M + m(\sin\sin\theta)^2\right]} \end{bmatrix} u \end{aligned} \tag{9}$$

The control goal is to set the controller u to quickly track the expected value (such as collar deflection) and suppress the perturbation effect. To facilitate the control of the design, (sinsin$\theta \approx \theta$, coscos$\theta \approx 1$, $\dot{\theta}^2 \approx 0$) is linearized near the equilibrium point $\theta \approx 0$.

The system dynamics equations can be updated, as shown in

$$(M+m)\ddot{x} + ml\ddot{\theta} = F\,, \tag{10}$$

$$ml^2\ddot{\theta} + ml\ddot{x} - fl\theta = 0\,. \tag{11}$$

The form of the linearized state space equation is

$$\dot{z} = Az + Bu\,, \tag{12}$$

where A is the system matrix, which describes the natural evolution of state, and B is the input matrix, which describes how the control inputs affect the state.

Equation (12) can be rewritten in the form of a matrix as follows.

$$\dot{z} = \frac{d}{dt}\begin{bmatrix} x & \theta & \dot{x} & \dot{\theta} \end{bmatrix} = \begin{bmatrix} \dot{x} & \dot{\theta} & \dfrac{mg}{M}\theta & \dfrac{(M+m)g}{Ml} \end{bmatrix} + \begin{bmatrix} 0 & 0 & \dfrac{1}{M} & \dfrac{1}{Ml} \end{bmatrix} u \tag{13}$$

The second derivative reflects the rate of change of the system state (position, angle) over time and is the core equation of the prediction model, as shown in Fig. 3. The results allow for better description and prediction of the future state of the system, i.e., $z_{k+1} = A_k Z_k + B_k u_k$, numerical integration (solve_ivp) to update the state and then design the controller.

The core idea of MPC is to solve a constrained optimization problem online over a finite prediction horizon. The key design elements include the selection of the prediction horizon N_p, control horizon N_c, weighting matrices Q and R, and the specifications of input and state constraints (e.g., air pressure, voltage limits, and deformation boundaries). In this study, the

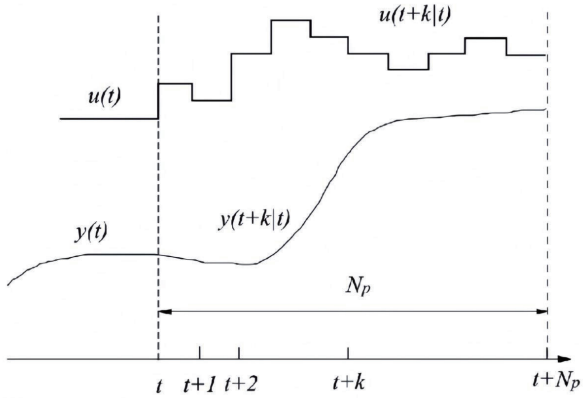

Fig. 3. Establishment of prediction model.

MPC parameters were determined through empirical tuning to balance deformation tracking accuracy, control smoothness, and computational efficiency. The prediction and control horizons were set to moderate values to provide sufficient future state information while maintaining real-time feasibility. The weighting matrix Q was adjusted to improve the deformation tracking performance, whereas R was selected to penalize excessive control effort and ensure smooth actuation. Using a finite-horizon receding optimization strategy, the quadratic cost function is defined as

$$J = \sum_{i=1}^{N_p} \| z_{k+i} - z_{ref} \|_Q^2 + \sum_{j=0}^{N_c-1} \| u_{k+j} \|_R^2 , \tag{14}$$

where $N_p = 10$ is the predicted value of the step size, $N_c = 10$ is the controlled value of the step size, the state error weighted matrix $Q = diag(100, 1, 1000, 1)$ emphasizes the position tracking accuracy and deformation suppression, and the control energy consumption matrix $R = 0.1$ limits the control input amplitude within the range of [10, −10] to avoid excessive control costs. The optimization process is generally performed to minimize or maximize an objective function.

Therefore, the constraints are defined as $u_{min} \le u \le u_{max}$, and the system state z_0 and control sequence $U = [u_0, u_1, ..., u_{N-1}]$ (the initial value can be zero or the historical optimal solution) are initialized. All comparative experiments were conducted under the same MPC parameter settings to ensure a fair evaluation. Sensitivity analysis through preliminary tuning indicated that moderate variations in these parameters did not alter the overall performance trend, and the reported improvements primarily reflect the intrinsic advantages of the control strategy rather than specific parameter choices.

The biggest advantage of rolling time domain optimization is that it has strong dynamic adaptability when the soft tool end effector touches the human tissue. If the external force increases linearly with the tissue deformation or changes abruptly, MPC can recalculate the optimal control quantity at each time step and dynamically adjust the air pressure input to suppress the deflection angle error. Optimal control is often difficult to determine effectively in the face of complex nonlinearities and constraints, and MPC considers the limited future time step to balance and computational efficiency, making the problem more manageable and adaptable. Therefore, MPC can effectively handle system constraints and multivariate control problems. In the control of soft robots, MPC can calculate the optimal control input in real time in accordance with the current system state, so as to achieve the precise control of the declination angle of the surgical tool and make it as close to 0 as possible to improve the accuracy and safety of surgery.

At each sampling moment k, the prediction deviation between the predicted output $y_m(k)$ of the model and the actual output $y(k + i)$ is

$$e(k+i) = y(k+i) - y_m(k) . \tag{15}$$

In the process of MPC policy execution, when the control process advances to the next sampling time, the actual output information of the system needs to be collected first. Using the

actual output data obtained, the prediction output results based on the system model can be dynamically corrected by calculating the deviation between it and the predicted output of the model. Subsequently, a new round of optimization calculation is carried out using the corrected forecast information.

3. Experimental Results

3.1 Experimental setup

In the experiments, the SciPy library was employed for numerical computation and optimization. Specifically, solve_ivp in the integrate module was used to solve the time-varying nonlinear differential equations; solve_continuous_are in the linalg module was adopted to compute the continuous-time algebraic Riccati equation; and minimize was applied to address the receding-horizon optimization problem within the MPC framework. Standard numerical configurations and default solver settings were retained to ensure numerical stability, reproducibility, and implementation consistency. To guarantee a fair comparison, both MPC and PID controllers were implemented using the same dynamic model, identical sampling time, and equivalent disturbance scenarios. Thus, the observed performance differences can be primarily attributed to the intrinsic characteristics of the control strategies rather than to numerical solver configurations. The dynamic bending model of the minimally invasive tool end effector was selected as the controlled object. A double closed-loop comparative platform for MPC and PID control was constructed to evaluate control performance under time-varying conditions, focusing on trajectory tracking and disturbance rejection. Two representative disturbance scenarios were designed to assess robustness: (1) a linearly time-varying external force, $d(t) = at + b$, and (2) a discretely time-varying external force, as illustrated in Fig. 4.

The evaluation indicators were selected to compare the control effects of six sets of comparison charts, namely, angle convergence, control input, end effector position, phase plane, error integration index, and anti-interference performance.

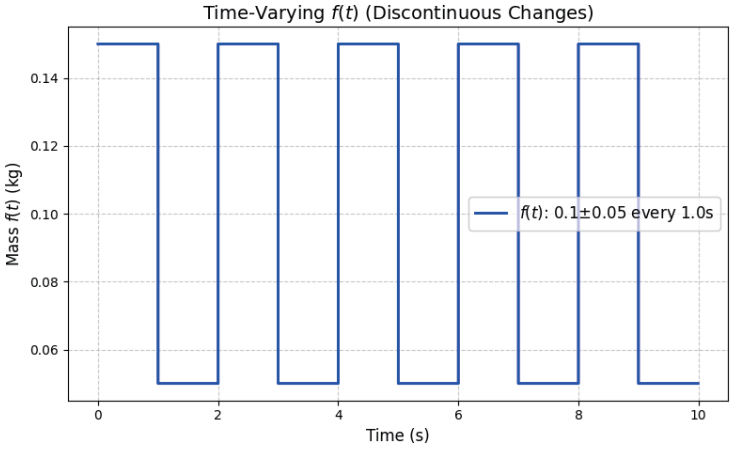

Fig. 4. (Color online) $M(t)$ diagram of the change in external force with runout.

3.2 Continuous linear change scenario of external force with time

Figures 5 and 6 show the performances of PID control and MPC in terms of angular convergence and x-position control of the minimally invasive tool end effector. The evaluation is based on time-domain performance metrics including settling time, overshoot, and oscillation amplitude.

Under PID control, the angular response exhibits high-frequency, large-amplitude oscillations, accompanied by noticeable overshoot and prolonged settling time. The x-position response also shows pronounced fluctuations, indicating limited damping capability and reduced transient stability. In contrast, MPC achieves angle convergence within approximately 1 s with significantly smaller oscillation amplitude and negligible overshoot. The corresponding position response is smoother and stabilizes more rapidly. These quantitative time-domain characteristics—namely shorter settling time, reduced overshoot, and lower oscillation amplitude—demonstrate that MPC provides faster convergence and enhanced closed-loop stability compared with PID control. Such improvements confirm the suitability of MPC for high-precision minimally invasive applications.

Using Figs. 7 and 8, we compare the performances of PID control and MPC in controlling input u and the angular error integral of the minimally invasive tool end effector. Under PID control, the input exhibits a large initial negative jump followed by rapid oscillations from −400 to 200, indicating high overshoot and unstable response. The angular error integral also fluctuates around zero, resulting in substantial control error. In contrast, MPC maintains small, stable input variations and continuous negative growth in the error integral, reflecting precise and steady angle control. MPC achieves fast convergence to the target angle, avoids large oscillations, and provides superior accuracy and reliability compared with PID control, making it more suitable for time-varying and high-precision surgical applications.

Figure 9 shows the phase trajectories under PID and MPC control strategies. The horizontal axis represents the angular displacement (rad), ranging from −3 to 3 rad/s, while the vertical axis denotes the angular velocity (rad/s), ranging from −30 to 30 rad/s. From a phase-plane

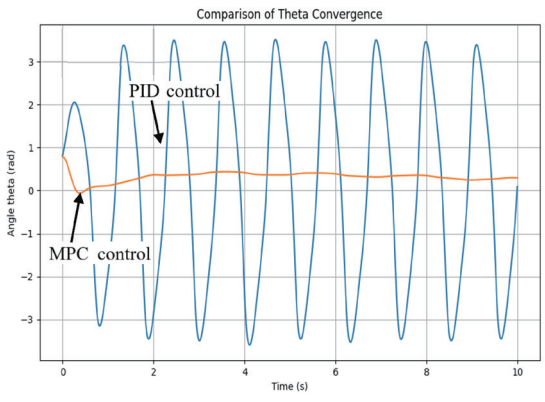

Fig. 5. (Color online) Angular convergence under linearly varying force.

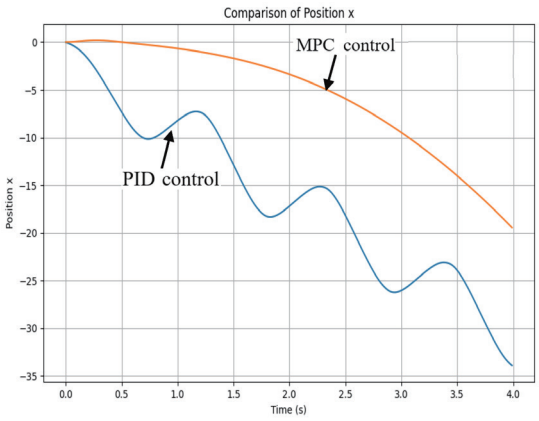

Fig. 6. (Color online) End-effector position of the minimally invasive tool under linearly varying force.

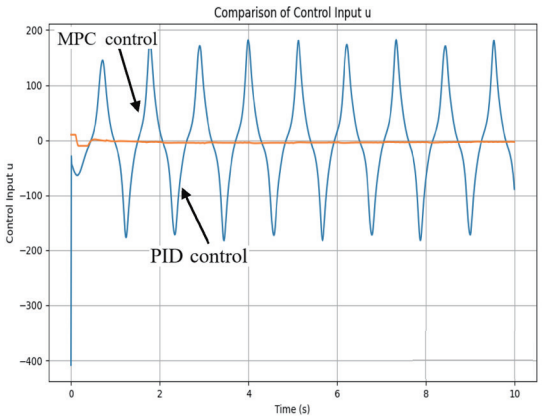

Fig. 7. (Color online) Control input U under a linearly varying force.

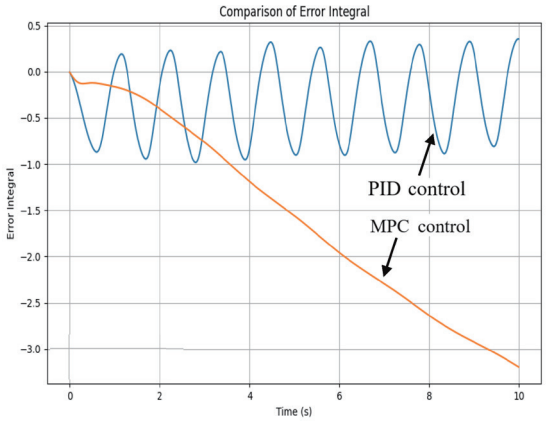

Fig. 8. (Color online) Integrated angular error under a linearly varying force.

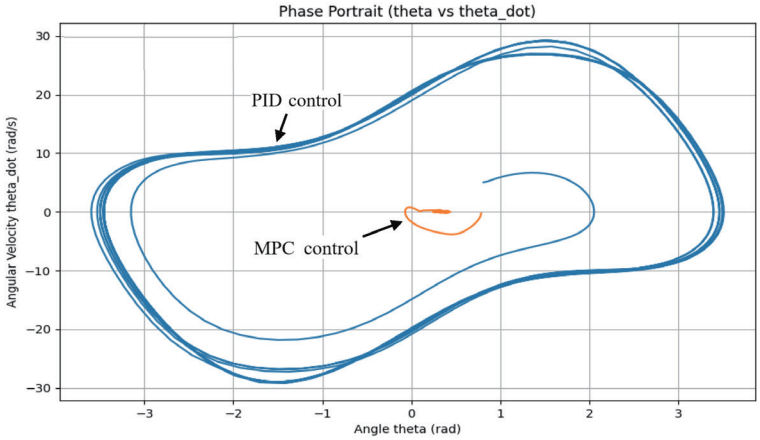

Fig. 9. (Color online) Phase trajectories under linearly varying force.

perspective, system stability and convergence characteristics can be evaluated by observing the trajectory shape, the number of loops, and the compactness of the path toward the equilibrium point. Under PID control, the phase trajectory exhibits a complex multiloop pattern with widely spread orbits. Such behavior indicates repeated oscillations and significant state deviations before convergence. The large enclosed area and multiple revolutions around the equilibrium point reflect insufficient damping and slower energy dissipation, resulting in prolonged settling time and relatively poor transient stability. In contrast, the phase trajectory under MPC control is more compact and contains fewer loops. The trajectory approaches the equilibrium point along a smoother and more direct path, with smaller deviations in both angular displacement and angular velocity. The reduced spiral amplitude and limited orbit expansion indicate improved damping characteristics and faster attenuation of oscillatory behavior. These features demonstrate enhanced transient stability and faster convergence to the equilibrium state under MPC control. Overall, the qualitative phase-plane characteristics—namely, the reduction in oscillatory loops, smaller trajectory dispersion, and more direct convergence path—confirm that MPC achieves superior stability and convergence performance compared with PID control.

In Fig. 10, we show the anti-interference performance of the minimally invasive tool end effector under PID and MPC control. The horizontal axis represents time (s), and the vertical axis shows the declination angle (rad). Under PID control, the declination angle exhibits large, frequent oscillations between approximately −3 and 3 rad/s, indicating that the system cannot quickly or stably adjust to 0 under time-varying interference. This highlights the limitations of PID in handling dynamic disturbances and its insufficient stability and anti-interference capability. In contrast, MPC maintains a smoother trajectory with small fluctuations around 0 rad. By predicting future disturbances and planning optimal control inputs, MPC effectively suppresses oscillations and stabilizes the declination angle. These results demonstrate the superiority of MPC in managing time-varying interference and provide a more reliable strategy for the precise deformation control of soft robots.

3.3 Scene of discrete runout change of external force with time

From Figs. 11 and 12, we show the performances of PID control and MPC for angular convergence and x-position control of the minimally invasive tool end effector. Under PID control, angles and positions exhibit large oscillations, with angles ranging from −25 to 15 rad/s, reflecting unstable and fluctuating system responses. In contrast, MPC control effectively suppresses early-stage oscillations, enabling rapid and stable convergence to the target angle and position. The end-effector position under MPC changes smoothly toward the desired value, maintaining stability throughout the control period. These results demonstrate that MPC achieves faster, more accurate, and more reliable control than PID, highlighting its suitability for the precise and stable manipulation of minimally invasive surgical tools.

We compare the performances of PID control and MPC in controlling input u and the angular error integral, shown in Figs. 13 and 14. Under PID control, the control input exhibits large negative jumps and rapid oscillations from −400 to 200, resulting in high overshoot and unstable response. The angular error integral also shows complex fluctuations and large deviations, reflecting low accuracy and poor system stability. In contrast, MPC control maintains small, smooth input variations and suppresses oscillations effectively. The error integral under MPC

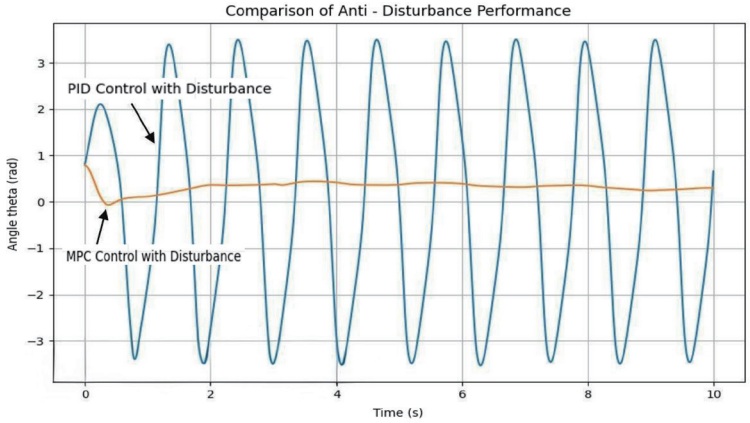

Fig. 10. (Color online) Anti-interference performance under linearly varying force.

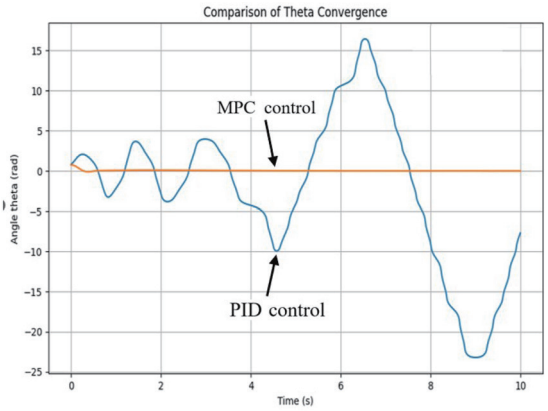

Fig. 11. (Color online) Angular convergence under runout variation.

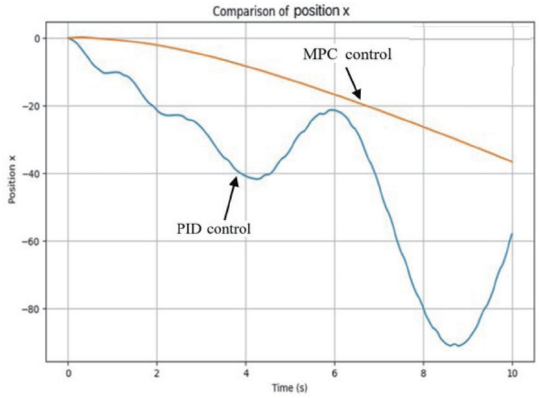

Fig. 12. (Color online) End-effector position under minimally invasive tool runout variation.

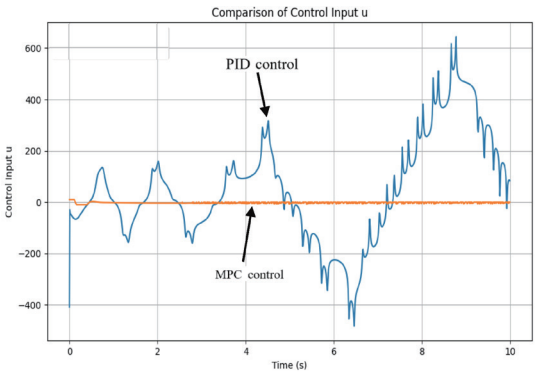

Fig. 13. (Color online) Control input U under runout variation.

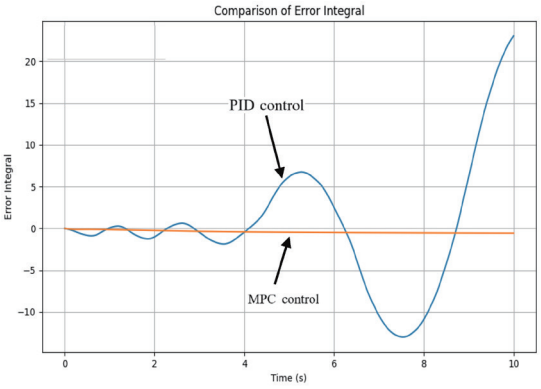

Fig. 14. (Color online) Integrated angular error under runout variation.

control remains close to zero, demonstrating fast, accurate, and stable control. These results verify the superiority of MPC over PID control in achieving precise and reliable performance.

Next, we compare the performances of PID control and MPC in controlling the angle and angular velocity of the minimally invasive tool end effector, shown in Figs. 15 and 16. In Fig. 15, PID control shows widely distributed phase trajectories with large angle and velocity ranges, indicating divergence and instability. In contrast, with MPC, phase trajectories are concentrated near 0 rad with small angular velocities, demonstrating stable convergence. Figure 16 illustrates the anti-interference performance, where PID control yields large oscillations from −20 to 40 rad/s, while MPC effectively suppresses interference and maintains the desired angle. These results highlight the superior stability, convergence, and robustness under MPC control compared with PID control.

3.4 VAEs

The core of VAE is mainly composed of three parts. (1) Encoder: It maps the input data X into a latent space and outputs the output parameters of the latent variable z. This process can be

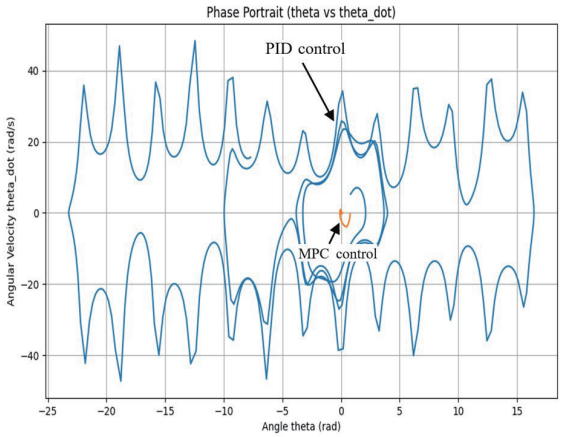

Fig. 15. (Color online) Phase trajectories under runout variation.

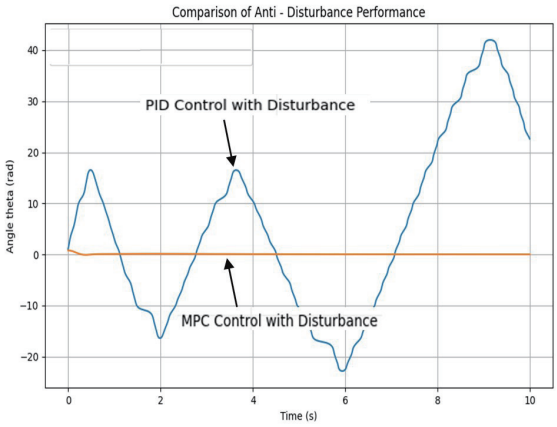

Fig. 16. (Color online) Anti-interference performance under runout variation.

expressed by a mathematical formula $Encoder(X) \rightarrow (u, \sigma)\sigma$, where the sum of u is the mean and standard deviation of the latent variables. (2) Latent Space: This is a form of low-dimensional representation used to learn data, generally continuous and regularized, close to the standard Gaussian distribution, i.e., $N \sim (u, \sigma^2)$. (3) Decoder: This generates new samples from the sampling of the latent space. This process can be expressed by the mathematical formula $Decoder(z) \rightarrow X'$, where X' is the reconstructed data. The specific network architecture design of VAE is shown in Fig. 17.

Therefore, to generate data or calculate gradients, sampling has become a key step in realizing the generation of data from latent space, and its core technique is reparameterization. The VAE algorithm can be divided into two processes: forward propagation and backpropagation.

(1) Forward pass:

The input sample X is encoded to generate the distribution parameters of latent variable z. Both the encoder and decoder use multilayer fully connected networks with ReLU activations. Assuming z follows a Gaussian distribution, auxiliary noise ε is introduced to isolate randomness, sampled from a standard normal distribution as shown below.

$$z = \mu + \sigma * \varepsilon \tag{16}$$

The latent variable z is generated through the reparameterization process.

(2) Backward pass:

The error between the loss function calculation model predicts the error between the predicted output and the actual output, and then propagates the error backwards from the decoder to the encoder to minimize the error. Backpropagation calculates gradients and updates the network through the chain law. The loss function is used to calculate the gap between the predicted output and the actual output. The reconstruction error measures the difference between the reconstructed data X' and the original data X, and the reconstruction loss function is shown in Eq. (17) using the mean error (*MSE*).

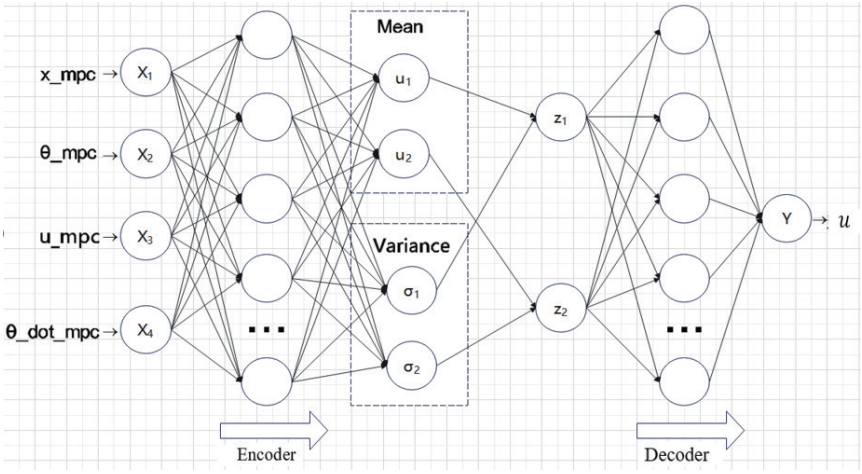

Fig. 17. Architecture of the proposed VAE module, where u is the generated control-parameter sequence serving as the initial control pattern.

$$\mathcal{L}_{recon} = \| X - X' \|^2 \tag{17}$$

KL divergence is a measure of the difference between the distribution of the hidden variable z and the standard state distribution, and the loss function of KL divergence is shown as follows.

$$\mathcal{L}_{KL} = \frac{1}{2} \sum \left(1 + \log\log\sigma^2 - \mu^2 - \sigma^2 \right) \tag{18}$$

Therefore, the total loss function is

$$\mathcal{L}_{VAE} = \mathcal{L}_{recon} + \beta \mathcal{L}_{KL}, \tag{19}$$

where β is used to adjust the weight of KL divergence.

The loss is backpropagated along the network while calculating the contribution of each parameter to the loss. Then, the optimization algorithms such as gradient descent are used to update the parameters to minimize the sum of the reconstruction error and KL divergence.

3.5 Model establishment and training

In essence, a well-trained VAE model enables the accurate representation of control parameters, thereby enhancing the precision of the surgical-tool deformation controller. The key hyperparameters considered in this study include the latent space dimension, encoder–decoder network architecture, learning rate, batch size, and number of training epochs. The hyperparameters were determined through systematic empirical evaluation based on three

criteria: reconstruction error, convergence behavior of the training loss, and stability of the generated control parameters when integrated into the MPC framework. In particular, the latent space dimension directly affects the representation capacity of the learned low-dimensional manifold. A dimension that is too small may fail to capture the essential features of the control parameter distribution, whereas an excessively large dimension may introduce redundancy and increase the risk of overfitting. Through comparative experiments with different latent dimensions, a two-dimensional latent space was found to provide an appropriate balance between expressive capability and generalization performance. It achieved low reconstruction error while maintaining stable control performance in subsequent MPC simulations. Both the encoder and decoder adopt a two-layer fully connected architecture with ReLU activation functions, which effectively capture the nonlinear characteristics of the control data without introducing unnecessary model complexity. The learning rate was set to 0.001 to ensure stable convergence; excessively large values caused oscillatory training behavior, while smaller values significantly slowed convergence. A batch size of 64 was selected to balance computational efficiency and gradient stability.

The number of training epochs was determined by analyzing the training and validation loss curves (Fig. 18). When the training process reached approximately 200 epochs, the reconstruction loss and Kullback–Leibler divergence stabilized, showing no further significant improvement. Further training led to marginal gains and potential overfitting. Therefore, 200 epochs was adopted as the final training setting. To ensure fair and consistent evaluation, all reported control experiments were conducted using the same trained VAE model and identical control framework settings. Consequently, the observed control performance primarily depends on the learned latent representation of the control parameters rather than minor variations in hyperparameter configurations. Additional fine-tuning experiments confirmed that small perturbations around the selected hyperparameter values did not significantly affect the robustness or stability of the closed-loop control performance.

Therefore, by continuously adjusting the control parameters and training the model, the VAE model can accurately learn the relationship between MPC control data and control strategy, and

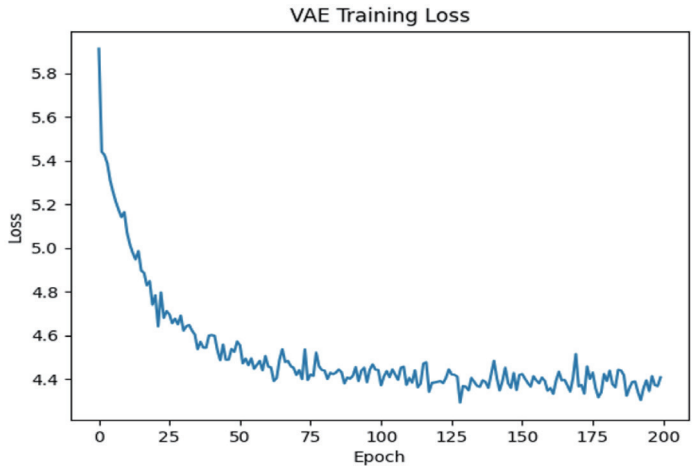

Fig. 18. (Color online) Loss curve of VAE model training.

provide accurate control input for subsequent MPC. During the training process, the hyperparameters are fine-tuned in accordance with the performance indicators on the validation set, such as adjusting the learning rate and changing the network structure, to further improve the performance of the model. After multiple rounds of training and adjustment, when the reconstruction error and Kullback–Leibler divergence of the model on the validation set reach a satisfactory level, the model is considered successful and can be used for subsequent deformation control tasks.

3.6 Comprehensive experimental verification

Through the deep integration of the VAE and MPC, precise deformation control of the minimally invasive tool under time-varying contact forces is achieved. The proposed framework establishes a learning-to-control coupling mechanism in which offline probabilistic learning enhances online control optimization.

First, the VAE is trained offline using MPC control data to capture the underlying distribution and structural features of optimal control sequences. The learning metrics reported in Table 2, including reconstruction accuracy and divergence measures, are used to evaluate the VAE's ability to faithfully represent control-relevant information. Higher learning accuracy and stable convergence indicate that the latent space effectively encodes essential control characteristics. This compact and structured representation serves as a probabilistic prior for MPC optimization.

By incorporating the learned latent representation into the MPC framework, the search space of online optimization is regularized and constrained toward meaningful control solutions. This reduces optimization variability and improves the consistency and smoothness of generated control inputs. As a result, the closed-loop system exhibits improved convergence speed, reduced oscillation amplitude, and enhanced stability.

Second, the MPC framework is designed to address the limitations of traditional PID control in handling time-varying disturbances. The effectiveness of the VAE-enhanced MPC strategy is further validated through comparative simulations between VAE-MPC and pure MPC in terms of position regulation and angular convergence, as shown in Figs. 19–22. The observed improvements in tracking performance and stability demonstrate that better VAE learning performance, as reflected by the metrics in Table 2, directly contributes to enhanced closed-loop control behavior.

Thus, the reported learning metrics are not only indicators of model training quality but also predictors of control performance improvement within the proposed VAE–MPC integrated framework. As shown in Fig. 23, it can be seen that the fusion control strategy of VAE-MPC effectively reduces the energy consumption required for pure MPC control. This confirms the effectiveness of VAE learning and shows the advantages of the VAE-MPC fusion control strategy compared with the pure control strategy.

Table 2
Model learning ability evaluation.

Learning model	Accuracy	Precision	Recall
VAE	0.935	0.901	0.865

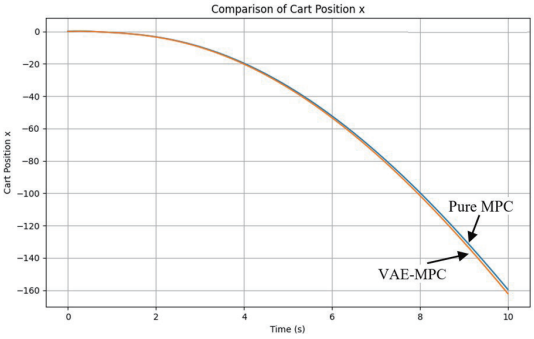

Fig. 19. (Color online) End-effector position of the minimally invasive tool under VAE-MPC and pure MPC.

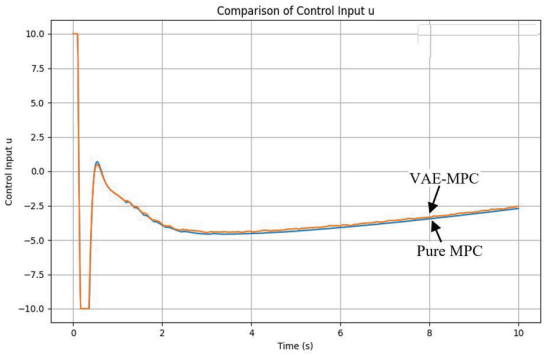

Fig. 20. (Color online) Control input u under VAE-MPC and pure MPC.

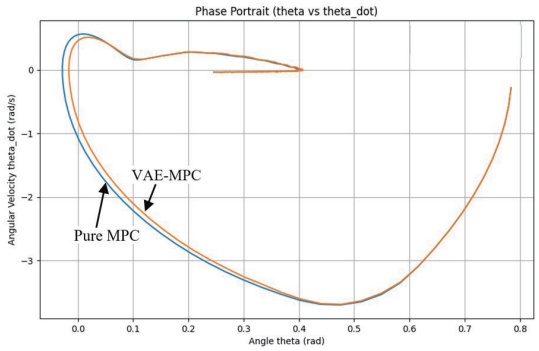

Fig. 21. (Color online) Phase trajectories under VAE-MPC and pure MPC.

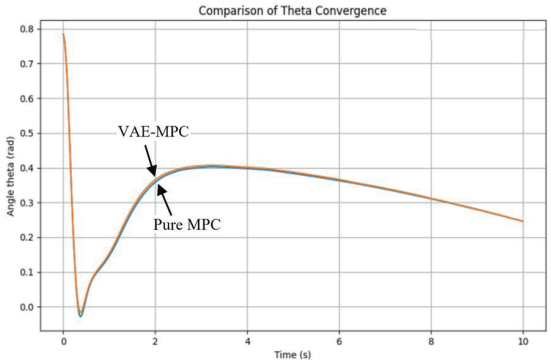

Fig. 22. (Color online) Angular convergence under VAE-MPC and pure MPC.

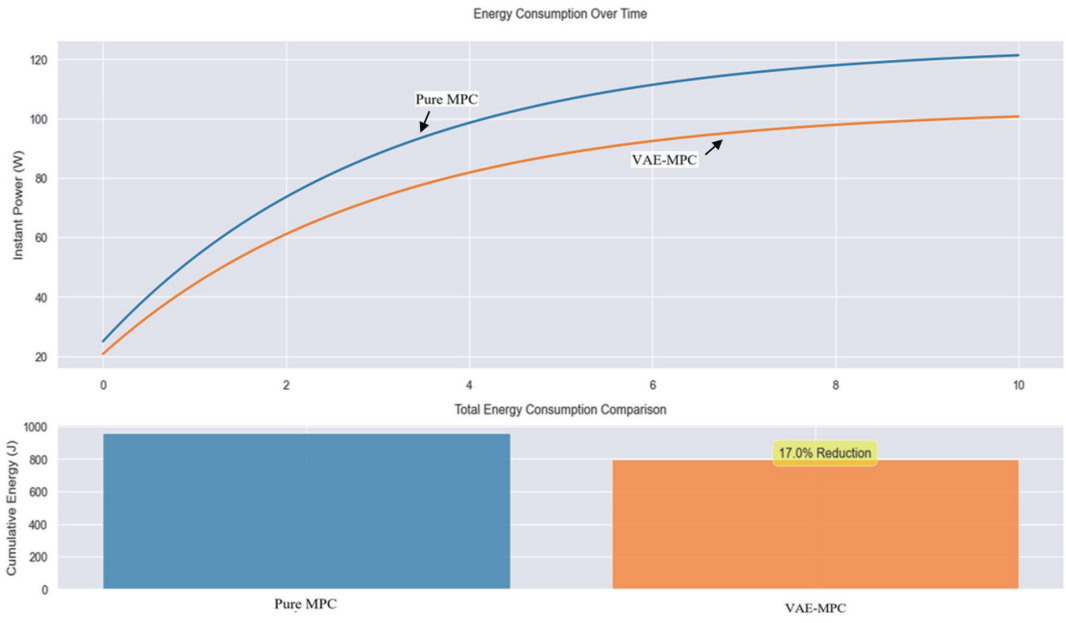

Fig. 23. (Color online) Energy consumption control under VAE-MPC and Pure MPC.

4. Conclusions

The MPC in VAE-MPC can achieve higher control accuracy than PID control when handling time-varying problems. The control input obtained with MPC is smoother and more stable than that obtained by PID control, and the energy consumption of its input is 1/6 of the energy consumed in PID control. For the scenarios of continuous change and discrete change of external force, MPC has a better control effect than PID control. By incorporating the VAE, VAI-SDC can considerably reduce the computational amount of MPC online optimization and reduce the computation time and energy consumption. From the experimental results, the total energy consumption of the fusion control strategy of VAE-MPC is reduced by about 17% compared with the that of pure MPC control. By combining the VAE model with the generated optimal control input, the effectiveness of the VAE-MPC fusion control strategy for the precise deformation control of minimally invasive tools can be obtained. Our experimental results demonstrate that VAI-SDC can stably provide precise and energy-efficient deformation control of surgical instruments, thereby enhancing clinical safety in various dynamic environments.

References

1 Y. Dong and B. Li: Appl. Sci. **13** (2023) 9430. https://doi.org/10.3390/app13169430
2 F. Xu, D. Ning, W. Hongtao, D. Longwei, and X. Shaohui: China Mech. Eng. **31** (2020) 1108. https://qikan.cmes.org/zgjxgc/EN/10.3969/j.issn.1004-132X.2020.09.013
3 D. P. Kingma and M. Welling: arXiv:1312.6114 (2022). https://arxiv.org/pdf/1312.6114
4 B. Kim, S. Shin, and H. Jung: Appl. Sci. **9** (2019) 2699. https://doi.org/10.3390/app9132699
5 S. M. Mohammad, X. Fu, J. Huang, and Md. A. Masud: Communications in Computer and Information Science. Data Mining (2018) 30. https://doi.org/10.1007/978-981-13-6661-1_3
6 G. Boquet, J. L. Vicario, A. Morell, and J. Serrano: ICASSP 2019- IEEE Int. Conf. Acoustics (IEEE, 2019) 2882. https://doi.org/10.1109/ICASSP.2019.8683011
7 H. Kameoka, L. Li, S. Inoue, and S. Makino: Neural Comput. **31** (2019) 1891. https://doi.org/10.1162/neco_a_01217
8 H. H. J. Bloemen, T. J. J. Van Den Boom, and H. B. Verbruggen: AIChE J. **50** (2004) 1453. https://doi.org/10.1002/aic.10122
9 Y. Lou, G. Hu, and P. D. Christofides: AIChE J. **54** (2008) 2065. https://doi.org/10.1002/aic.11511
10 M. Mahmood and P. Mhaskar: 2008 American Control Conf. (IEEE, 2008) 1487. https://doi.org/10.1109/ACC.2008.4586645
11 R. F. Shepherd, F. Ilievski, W. Choi, and G. M. Whitesides: Proc. National Academy of Sciences of the United States of America (2011) 20400. https://doi.org/10.1073/pnas.1116564108
12 T. Ranzani, G. Gerboni, M. Cianchetti, and A. Menciassi: Bioinspiration Biomimetics **10** (2015) 035008. https://iopscience.iop.org/article/10.1088/1748-3190/10/3/035008
13 Y. Huan, I. Tamadon, C. Scatena, V. Cela, A. G. Naccarato, and A. Menciassi: IEEE Trans. Biomed. Eng. **68** (2021) 56. https://doi.org/10.1109/tbme.2020.2996965
14 J. E. A. Wickham: Br. Med. J. **295** (1987) 1581. https://doi.org/10.1136/bmj.295.6613.1581
15 J. Zhou, S. Chen, and Z. Wang: IEEE Rob. Autom. Lett. **2** (2017) 2287. https://doi.org/10.1109/LRA.2017.2716445